Engineering Analysis with Boundary Elements 35 (2011) 489–494

Contents lists available at ScienceDirect

Engineering Analysis with Boundary Elements

journal homepage: www.elsevier.com/locate/enganabound

BEM simulations of potential flow with viscous effects as applied to a rising bubble

Evert Klaseboer [a], Rogerio Manica [a], Derek Y.C. Chan [b,c], Boo Cheong Khoo [d,*]

[a] Institute of High Performance Computing, 1 Fusionopolis Way, #16-16 Connexis, Singapore 138632, Singapore
[b] Particulate Fluids Processing Centre, Department of Mathematics and Statistics, The University of Melbourne, 3010, Australia
[c] Department of Mathematics, National University of Singapore, Singapore 117543, Singapore
[d] Department of Mechanical Engineering, National University of Singapore, Singapore 117576, Singapore

ARTICLE INFO

Article history:
Received 7 October 2008
Accepted 9 September 2010

Keywords:
Transient bubble rise and deformation
Boundary element method
Terminal velocity
Drag force

ABSTRACT

A model for the unsteady rise and deformation of non-oscillating bubbles under buoyancy force at high Reynolds numbers has been implemented using a boundary element method. Results such as the evolution of the bubble shape, variations of the transient velocity with rise height and the terminal velocity for different size bubbles have been compared to recent experimental data in clean water and to numerical solutions of the unsteady Navier–Stokes equation. The aim is to capture the essential physical ingredients that couple bubble deformation and the transient approach towards terminal velocity. This model requires very modest computational resources and yet has the flexibility to be extended to more general applications.

1. Introduction

Results of experiments pertaining to bubble rise in a variety of liquids and liquid mixtures have been reviewed recently by Loth [1]. Magnaudet and Eames [2] summarised various theoretical and empirical approaches to the problem of bubble motion at high Reynolds numbers. The focus of this paper is on modelling the behaviour of rising bubbles in clean water for equivalent bubble diameters up to ~ 4 mm or Reynolds number up to ~ 1000. The aim is to predict the transient rise velocity and corresponding deformation of initially spherical bubbles under the influence of buoyancy forces. The well-known summary of terminal velocity, U, versus equivalent bubble diameter, d, in clean and unpurified water of Clift et al. [3] (Fig. 1) provides a good visual overview. Also shown in this figure are theoretical results for a spherical bubble corresponding to the Hadamard–Rybczynski (HR) formula [4]: $U=4\rho g d^2/3\mu$ valid for Stokes flow; the Levich formula [5–7]: $U=4\rho g d^2/9\mu$ valid in the limit of infinite Reynolds number, $Re=\rho U d/\mu\to\infty$; and the empirical correlation formula given by Magnaudet and Eames [2] which has been constructed from the results of Mei et al. [8] and Moore [9] (together denoted as MM) to fit experimental data for spherical bubbles in the range $0\le Re\le 500$. Here ρ is the water density, μ the dynamic shear viscosity and g the gravitational acceleration. All these theoretical results assume the zero tangential stress boundary condition at the surface of a spherical bubble which is appropriate for experiments conducted in highly purified water. It is well known that rising bubbles in ultra clean water follow a rectilinear path until a critical equivalent diameter of about 2 mm when the terminal velocity attains a local maximum, and beyond which the bubble path can zig-zag or spiral. However, the terminal velocity in the rectilinear regime is very sensitive to even trace amounts of contamination so it is important to cross-validate experimental data from a number of independent sources and ascertain that the measurements are free from artifacts.

Recently, Malysa et al. [10] measured the transient rise of deformed bubbles of equivalent diameter between 1.35 and 1.43 mm (around the location of the velocity maximum in Fig. 1) in ultra clean water. The observed terminal velocity of 35 cm/s (which corresponds to a Reynolds number of about 500) is in excellent agreement with the experiments of Duineveld [11] and Wu and Gharib [12] who measured the terminal velocities of deformed bubbles in clean water in the range of equivalent diameters between 1 and 2 mm. These results are also consistent with the earlier measurements of Okazaki [13]. This range of bubble size is of particular significance in mineral flotation applications [14] and many other industrial processes.

With small amounts of added surfactants, Malysa et al. [10] reported that the terminal velocity for same sized bubbles fell to 15 cm/s, which again is in excellent agreement with the observations of Zhang and Finch [14] and of Wu and Gharib [12] for cases where the bubbles become contaminated by the bubble generation method. These small concentrations of added surfactants render the bubble surface immobile while the interfacial tension remains unaffected.

* Corresponding author.
E-mail address: mpekbc@nus.edu.sg (B.C. Khoo).

0955-7997/$ - see front matter © 2010 Elsevier Ltd. All rights reserved.
doi:10.1016/j.enganabound.2010.09.005

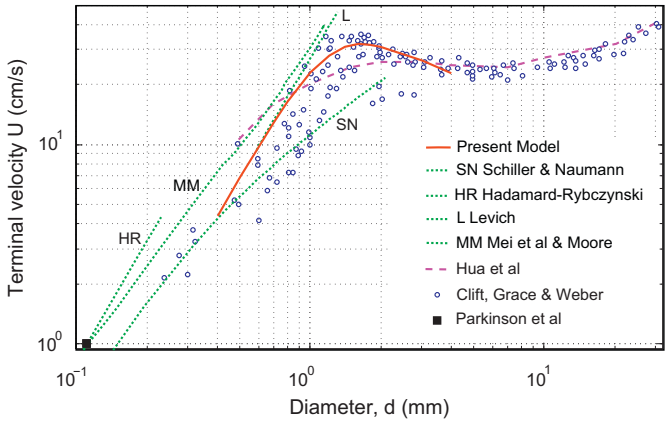

Fig. 1. Numerical results of the terminal velocity of deformable bubbles predicted by the present model and by the full 3D solution of the unsteady Navier–Stokes equation of Hua et al. are compared to experimental data summarised by Clift et al. [3]. Familiar theoretical results for spherical bubbles are also plotted. See text for details.

The results of three independent experimental studies by Duineveld, Malysa et al. and Wu and Gharib on the terminal oblate ellipsoidal shapes of bubbles in clean water as characterized by variations of the aspect ratio with equivalent bubble size are also in excellent agreement (see Fig. 2b). In the presence of surfactants or for contaminated bubbles, all three studies reported lower terminal velocities of the same magnitude ($Re \sim 200$) and the terminal bubble shapes remain nearly spherical. Therefore, one can be quite confident that these results represent the correct behaviour of rising bubbles in water under clean, contaminant free conditions. Taken together with the recent measurements of the rise of microbubbles in ultra clean water by Parkinson et al. [15], we have a complete and reliable experimental data set for the rectilinear rise of spherical and deformed bubbles in water for Reynolds numbers up to ~ 500.

Numerical modelling of unsteady rising bubbles using grid-based numerical methods that take into account deformations in a self-consistent way has been attempted using both an axi-symmetric boundary-fitted coordinate formulation [16,17] and a full three-dimensional solution [18,19] of the Navier–Stokes equation. Such approaches are quite complex to implement and are very demanding in terms of computational resources [20]. This places practical limitations on extending them to more complex and interesting multiphase problems [21] involving, for example the motion and deformation of multiple bubbles in response to external fields or to model dynamic interactions between bubbles and between bubbles and surfaces or interfaces. A relatively simple, yet accurate model that can accommodate these complexities at relatively high Reynolds numbers is therefore desirable [10].

A promising approach to treat bubble dynamics at high Reynolds number is via a boundary integral formulation that only uses the properties of the bubble surface to track its evolution. In addition to computational efficiencies conferred by the reduction of one spatial dimension, the focus on the boundary means that interactions between bubbles and surfaces that may involve short-ranged surface forces can be included without complex implementation issues associated with obtaining a sufficiently accurate resolution of a deforming air/water interface in grid-based computational schemes.

The boundary integral method has been used in the past to simulate models involving deformable rising bubbles. Miksis et al. [22] considered potential flow and obtained shapes and terminal velocities but did not consider transient behavior. Boulton-Stone et al. [23] and Blake et al. [24] considered the transient motion of one bubble or a pair of bubbles rising in the absence of viscosity effects and so did not address the question of terminal velocities.

The theory considered in this paper is motivated by the boundary integral formulation by Lundgren and Mansour [25], appropriate at high Reynolds numbers, to study weak viscous effects on the oscillation of a liquid drop in a gravity-free environment. However, for the rising bubble problem, we include a gravitational body force at the outset. The aim is to produce a theory that can describe the evolution of the position, velocity and deformations of the bubble surface in a self-consistent way. At high Reynolds number, the viscous potential flow approach [26] is able to predict the exact limiting forms of the terminal velocities of spherical and ellipsoidal bubbles using a viscous correction due to Joseph and Wang [27] for the viscous pressure. Here we extend this approach to estimate bubble deformations and transient effects. As we shall see, the self-consistent bubble shapes so obtained are close to perfect oblate ellipsoids, therefore we expect this approach will yield quantitatively correct results. The practical utility of this approach is illustrated by comparing predictions of this approach with experimental results summarized earlier.

2. Formulation

The velocity field $\mathbf{u}$ of an incompressible Newtonian fluid obeys the Navier–Stokes equation [28]

$$\rho\frac{\partial \mathbf{u}}{\partial t}+\rho\mathbf{u}\cdot\nabla\mathbf{u}=-\nabla p+\mu\nabla^2\mathbf{u}-\rho\mathbf{g} \tag{1}$$

and the conservation of mass condition $\nabla\cdot\mathbf{u}=0$, where p represents the pressure, t the time and $\mathbf{g}$ the body force acting on the fluid due to gravity. The boundary condition at the surface of the bubble is given by the Young–Laplace equation for which the difference in normal stress across the bubble surface is balanced by the product of the interfacial tension, σ and the local mean curvature, κ:

$$p_{in}-p+2\mu\frac{\partial u_n}{\partial n}=\sigma\kappa \tag{2}$$

where p_{in} is the internal pressure of the bubble, u_n is the normal component of the velocity and $\mathbf{n}$ is the unit outward normal directed into the fluid. In the above equation, $\partial/\partial n=\mathbf{n}\cdot\nabla$ represents the normal derivative. We also assume the bubble surface is fully mobile so that the tangential stress vanishes.

We employ the exact Helmholtz decomposition: $\mathbf{u}\equiv\mathbf{u_p}+\mathbf{v}=\nabla\phi+\mathbf{v}$, where $\mathbf{u}$ is written as a sum of an irrotational field, $\nabla\phi$ (with ϕ the velocity potential) and a rotational field, $\mathbf{v}$. Eq. (1) can then be recast as

$$\nabla\left\{\rho\frac{\partial\phi}{\partial t}+\frac{1}{2}\rho|\nabla\phi|^2+p+p_v+\rho gz\right\}=0 \tag{3}$$

where the viscous pressure, p_v is given by

$$\nabla p_v\equiv\rho\frac{\partial\mathbf{v}}{\partial t}+\rho(\mathbf{v}\cdot\nabla)(\nabla\phi)+\rho(\nabla\phi\cdot\nabla)\mathbf{v}+\rho\mathbf{v}\cdot\nabla\mathbf{v}-\mu\nabla^2\mathbf{v} \tag{4}$$

At high Reynolds numbers, the irrotational part of the velocity $\nabla\phi$ provides a uniformly valid leading order approximate solution to the velocity field so that $\partial u_n/\partial n\cong\partial^2\phi/\partial n^2$ [29]. The evolution of the potential and the position $\mathbf{X}$ of an element of the bubble

surface is governed by

$$\rho\frac{D\phi}{Dt}=\frac{1}{2}\rho|\nabla\phi|^2-2\mu\frac{\partial^2\phi}{\partial n^2}+\sigma\kappa-\rho gz-p_{in}-p_v+p_0(t) \tag{5}$$

$$\frac{D\mathbf{X}}{Dt}=\nabla\phi \tag{6}$$

Here $p_0(t)$ is the ambient pressure that can be time dependent in general and D/Dt is the material derivative: $D/Dt=\partial/\partial t+\mathbf{u_p}\cdot\nabla$. The form of the internal pressure of the bubble p_{in} depends on the choice of equation of state for the bubble, which may for example, be the isothermal or the adiabatic equation. The continuity condition for the liquid implies $\nabla^2\phi=0$ so that on the surface of the bubble we have the integral equation [30]

$$c\phi+\int_S\phi\frac{\partial G}{\partial n}\,dS=\int_S G\frac{\partial\phi}{\partial n}\,dS \tag{7}$$

with G the 3D Green function for the Laplace equation and c the solid angle.

Eqs. (5)–(7) now constitute a boundary integral formulation for the unsteady motion and deformation of a bubble that accounts for effects of buoyancy, inertia, viscous forces and surface tension effects.

Joseph and Wang [27] proposed a method to estimate the viscous pressure p_v at the bubble surface for high Reynolds numbers when the velocity field can be approximated by the potential flow solution $\mathbf{u_p}=\nabla\phi$. They argued that in order to satisfy the zero tangential stress boundary condition at the bubble surface, the viscous pressure p_v must compensate for the non-zero shear stress: $\tau_s=2\mu\mathbf{t}\cdot\nabla\mathbf{u_p}\cdot\mathbf{n}$, at the bubble surface that arises from the irrotational solution. This is expressed as an integral condition on the bubble surface:

$$-\int_S(\mathbf{u}_p\cdot\mathbf{n})p_v\,dS=\int_S(\mathbf{u}_p\cdot\mathbf{t})\tau_s\,dS \tag{8}$$

Joseph and Wang [27] derived this equation by calculating the kinetic energy in the fluid domain based on the Navier–Stokes equations. The rate of change of this energy is then considered and expressed in terms of surface integrals, taking into account that the shear stress vanishes on the bubble surface. They then continue to argue that the dissipation in potential flows does not vanish and gives rise to a viscous pressure contribution (which is basically a correction to the irrotational pressure term). Interested readers are referred to Joseph and Wang for more details.

For an axi-symmetric problem, p_v on the bubble surface can be expanded in terms of the surface harmonics. For our model, we retain only one term: $p_v\approx C_1\cos(\beta)$ where $0\le\beta<\pi$ is the normalised arc length of the bubble surface and the constant C_1 is then determined from (8).

Our aim is to model the experiments of Duineveld, Malysa et al. and Wu and Gharib by starting with a spherical bubble at rest and obtain a description of the transient behaviour as the bubble rises under buoyancy force to its terminal velocity and deforms into its final shape.

3. Numerical implementation

An axi-symmetric implementation of the boundary element method using a cylindrical coordinate system (r,z) is used to solve the governing Eqs. (5)–(8). The terms $\partial^2\phi/\partial n^2$ in (5) and τ_s in (8) can be obtained with the help of the Laplace equation as [22,25]

$$\frac{\partial^2\phi}{\partial n^2}=-\frac{n_z}{r}\frac{\partial\phi}{\partial s}-\kappa\frac{\partial\phi}{\partial n}-\frac{\partial^2\phi}{\partial s^2}=-\frac{n_z}{r}u_t-\kappa\frac{\partial\phi}{\partial n}-\frac{\partial u_t}{\partial s} \tag{9a}$$

$$\tau_s=2\mu\left[\frac{\partial u_n}{\partial s}+u_t\left(n_r\frac{\partial n_z}{\partial s}-n_z\frac{\partial n_r}{\partial s}\right)\right] \tag{9b}$$

with n_r and n_z the r and z components of the normal vector, u_t the tangential component of the velocity and s the arclength along the bubble surface. Furthermore, the curvature κ is obtained with $\tan\theta=dz/dr$ resulting in $\kappa=\sin\theta/r+d\theta/ds$ according to Chesters [31] which is equivalent to $\kappa=-n_r\partial n_z/\partial s+n_z\partial n_r/\partial s+n_r/r$.

The code we employ has been used extensively to study oscillatory bubble dynamics, such as in underwater explosions [32,33], micro-pumps [34], lithotripter shockwave–bubble interaction [35], accelerating particles due to cavitation [36] and bubbles in sound waves near biomaterials [37]. The N nodes on the bubble are distributed evenly along the surface. A node redistribution scheme, based on a cubic spline interpolation with respect to the arc length along the bubble surface, is applied to prevent the nodes from clustering as the bubble evolves. Furthermore smoothing is applied every 50 time steps using a five-point smoothing formula of Longuet-Higgins and Cokelet [38]. The position and potential at the next time step for each node are obtained from (5) and (6) as

$$\phi^{t+\Delta t}=\phi^t+\frac{\Delta t}{\rho}\left(\frac{1}{2}\rho|\nabla\phi|^2-2\mu\frac{\partial^2\phi}{\partial n^2}+\sigma\kappa-\rho gz-p_{in}-p_v+p_0\right)^t \tag{10}$$

$$\mathbf{X}^{t+\Delta t}=\mathbf{X}^t+\Delta t(\nabla\phi)^t \tag{11}$$

with Δt the time step, t the present time and $t+\Delta t$ the new time. Applying (7) for each node will give a $N\times N$ matrix equation to be solved for the unknown normal velocity. The velocity vector is obtained using this normal velocity and the potential distribution along the surface of the bubble (which will give the tangential velocity component). For more details on the numerical implementation see [39]. To calculate a bubble rising from rest to attain terminal velocity requires several minutes on a desktop general purpose computer. The initial conditions for the problem are taken as a spherical bubble at rest at $t=0$, with initial volume $V_0=\pi d^3/6$ and initial pressure $p_{in,0}=p_0+4\sigma/d$, with $p_0=p_0(t)=1$ bar. The time-step is taken to be $0.01d\sqrt{\rho/p_0}$. We assume the ideal adiabatic equation of state for the bubble: $p_{in}=p_{in,0}(V_0/V)^\gamma$ where $\gamma=\frac{5}{4}$, but the variation in the bubble volume V is less than 1% as it rises.

4. Results

The terminal velocity predicted by our model for equivalent bubble diameter, d, up to 4 mm is shown in Fig. 1 together with the collection of experimental data from Figure 7.3 of Clift et al. [3]. For $d>4$ mm bubbles no longer rise along a rectilinear path. At any bubble size, the scatter in the experimental terminal velocities is due to the presence of contaminants or surfactants in the water which lower the terminal velocity by varying degree. The curve labelled SN [40] corresponds to the empirical formula: $C_D=(24/Re)\,(1+0.15\,Re^{0.687})$ for the terminal velocity of a 'solid' sphere which obeys the no-slip rather than the zero tangential stress boundary condition. Also shown are results of calculations for deformable bubbles based on a full 3D solution of the unsteady Navier–Stokes equations by Hua et al. [18] which predicted terminal velocities lower than that observed in ultra clean water.

To demonstrate the effects of bubble deformation, we also show theoretical results for spherical bubbles valid at different ranges of the Reynolds number, Re, summarised by Magnaudet and Eames where the terminal velocity is given implicitly by the

relation $\pi\rho g d^3/6 = (\pi/8)C_D\rho U^2 d^2$, for $0 \le Re \le 500$, where C_D in the interpolation formula combines the result by Mei et al.

$$C_D = \frac{16}{Re}\left\{1+\left[\frac{8}{Re}+\frac{1}{2}\left(1+\frac{3.315}{Re^{1/2}}\right)\right]^{-1}\right\}, \quad 1 < Re < 50 \tag{12a}$$

and [9]

$$C_D = \frac{48}{Re}\left(1-\frac{2.21}{Re^{1/2}}\right), \quad Re \ge 50 \tag{12b}$$

For larger diameters, $d > 1.0$ mm and considering the absence of adjustable parameters, our high Reynolds number model agrees quite well with experimental data for clean bubbles (see Fig. 1). There is also agreement with the interpolation formula (12) for d between 0.4 and 1.0 mm where bubble deformation is not significant. For d below 0.4 mm, the Reynolds number becomes less than 30, and viscous effects become important which accounts for the deviation from (12).

In Fig. 2 we compare, on a linear scale, experimental results obtained independently by Duineveld, Malysa et al. and Wu and Gharib for bubbles in ultra clean water for which the zero tangential stress boundary condition applies. In the practical range of equivalent diameter, d between 0.5 and 2 mm, where bubble deformation is important ($50 < Re < 600$, based on the terminal velocity and equivalent bubble diameter), our model predicts the existence of the velocity maximum around the equivalent diameter of 1.5 mm, but underestimates experimental velocities by about 10% (Fig. 2a). This is due to the fact that in the limit of a non-deforming spherical bubble, our theory will give the Levich drag coefficient of $C_D = 48/Re$ which is an upper bound. By assuming bubbles deform as fore-aft symmetric oblate ellipsoids, Moore [41] derived a result for the drag coefficient C_D that included a correction of order $Re^{-3/2}$, and reduces to (12b) for spherical bubbles, and provides closer agreement with experiments. Using a boundary-fitted coordinate system, Yang et al. [17] solve the axi-symmetric Navier–Stokes equations for three bubble diameters between 0.72 and 1.2 mm and their results for the terminal velocities are in good agreement with experiments. Also shown in Fig. 2a is the empirical relation of the terminal velocity from Clift et al. [3]: $U = [(2.14\sigma/d) + 0.505gd]^{1/2}$ valid for $d > 1.1$ mm.

In Fig. 2b, we compare the degree of deformation as measured by the bubble aspect ratio corresponding to the terminal velocities in Fig. 2a. The present theory as well as that of Moore [41] and Yang et al. [17] are all in good accord with experiments. Over this size range, the deformed bubbles closely resemble oblate ellipsoids.

In Fig. 3a–d, we present an overview of predicted variations in bubble shape as spherical bubbles of different sizes are released from rest in clean water and allowed to rise towards terminal velocity and steady state deformed shape. Clearly our simple model has captured the physical essence that a rising bubble will begin to flatten when the pressure drop around the equator of the bubble due to the Bernoulli effect (ρU^2) can no longer balance the Laplace pressure ($4\sigma/d$) of the bubble. The resulting flattening then creates a larger cross-sectional area normal to the direction of bubble motion which increases the drag on the bubble. The balance between these two effects then gives rise to a steady state velocity and deformed shape. The deformation of the bubble is

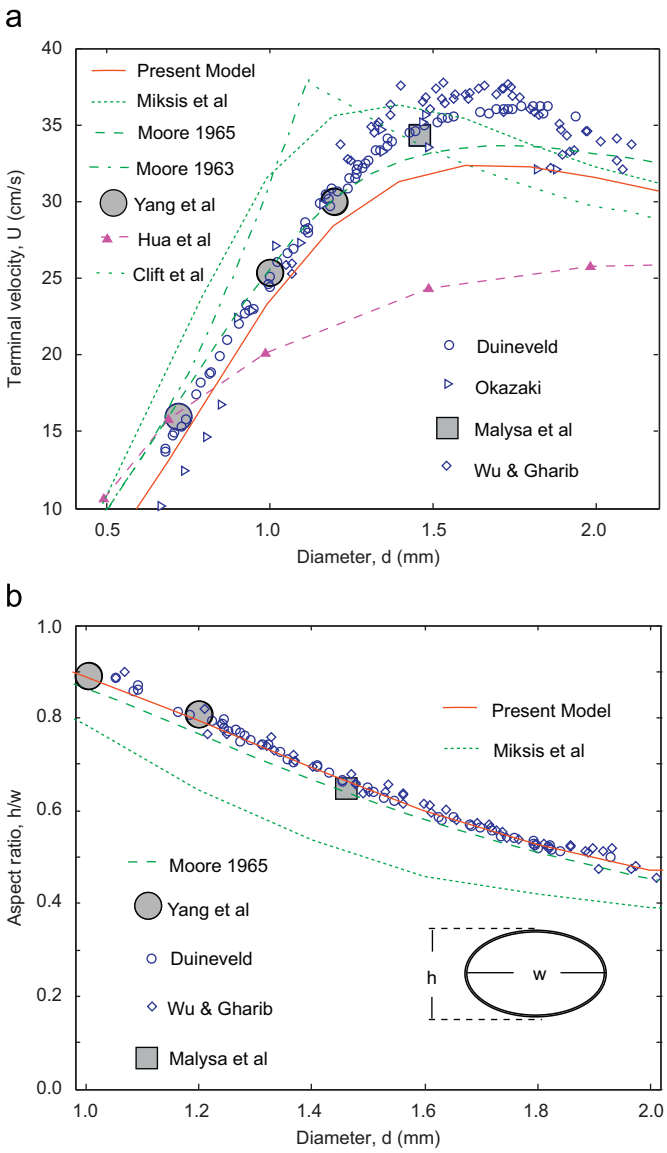

Fig. 2. Comparisons between results from the present model and other numerical, empirical and experimental results for the range of bubble diameters of practical interest: (a) the terminal velocity (b) the aspect ratio, h/w of the deformed bubble.

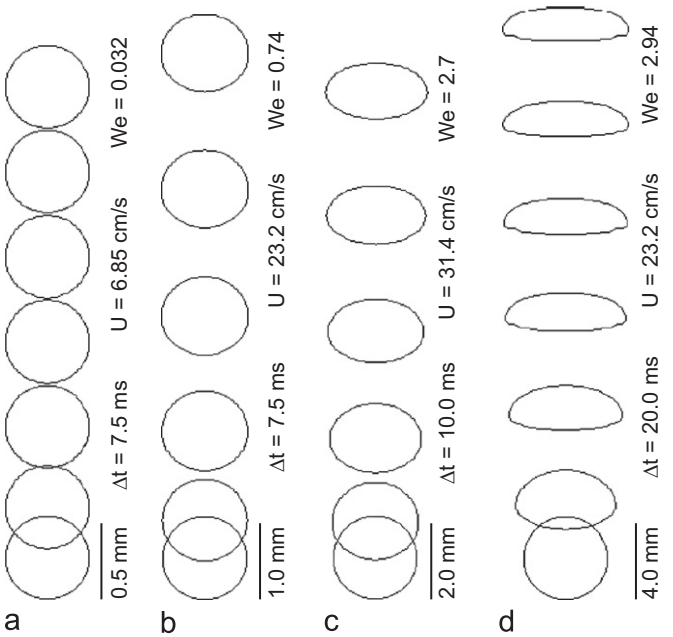

Fig. 3. (a–d) Theoretical evolution of bubble positions and shapes at the indicated time intervals Δt for initial diameters ranging from 0.5 to 4 mm. Physical inputs correspond to bubbles in clean water: $\sigma = 73$ mN m^{-1}, $\mu = 10^{-3}$ Pa s, $\rho = 1000$ kg m^{-3}.

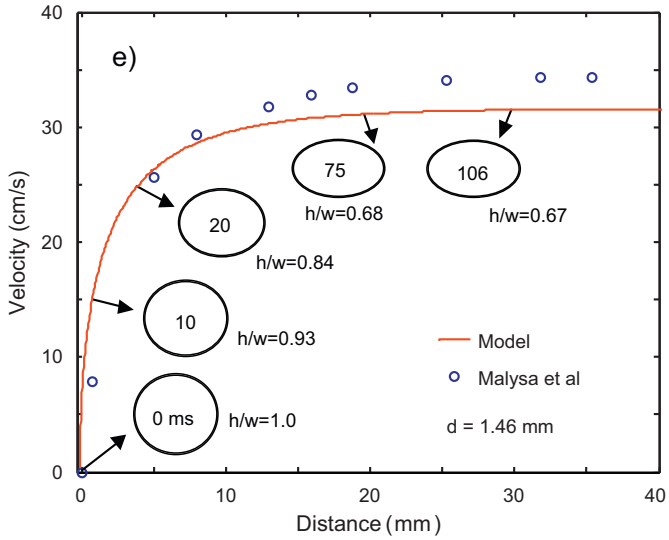

Fig. 4. Comparisons between the current model and time-dependent experiment of Malysa et al. [10] for the rise velocity as a function of the distance travelled from the point of release. The initially spherical bubble has diameter 1.46 mm. The corresponding elapsed times in milliseconds are indicated in each deforming bubble shape.

determined by the Weber number $We = \rho U^2 d/\sigma$. In Fig. 3a–d we see that the terminal shape of the bubble becomes an oblate ellipsoid as *We* exceeds unity.

In Fig. 4, we compare the prediction of our model with the experimental results of Malysa et al. [10] on the evolution in rise velocity and bubble shape as a spherical bubble (diameter 1.46 mm) is released from rest and allowed to rise and attain terminal velocity and shape. In this case, the Reynolds number based on the terminal velocity is around 500. This confirms that the present model is capable of predicting both steady state and transient behaviour of rising bubbles.

5. Discussion and conclusions

The current model is closely related to the Rayleigh–Plesset equation for the radius $R(t)$ of an oscillating spherical bubble [42,43]

$$p_{in} - \rho\left[\frac{3}{2}\left(\frac{dR}{dt}\right)^2 + R\frac{d^2R}{dt^2}\right] - \frac{2\sigma}{R} - p_0(t) - \frac{4\mu}{R}\frac{dR}{dt} = 0 \qquad (13)$$

in which viscous effects are included through the normal viscous stress jump condition at the interface via the last term on the left-hand side which corresponds to $2\mu(\partial u_n/\partial n)$ in (2). However, due to spherical symmetry, the shear stress and the viscous pressure term p_ν are absent. In the present model we use the idea suggested by Joseph and Wang [27] to estimate the p_ν contribution and this approach can be viewed as a generalised Rayleigh–Plesset model for oscillating and translating bubbles. Omitting the p_ν contribution will give the model of Miksis et al. [22] which predicts a smaller value of C_D (giving $C_D = 32/Re$ instead of $48/Re$ for spherical bubbles) and therefore overestimates the terminal velocity of deformed bubbles (see Fig. 2a) as well as the degree of deformation (see Fig. 2b).

The present model cannot account for the possibility of recirculation zones that can develop on the down-stream side of the bubble. However, we can see in Fig. 1 that because bubble deformation in clean water is significant at finite Reynolds number, the terminal velocity deviates from the Levich exact asymptotic result which applies to spherical bubbles. From a different perspective, the good agreement we observed with the present model would strongly suggest that the effects of such recirculation zones may only provide a small correction to the terminal velocity and final shape for bubbles in this size range. To predict the possibility of non-rectilinear motion observed for bubbles larger than about ~ 2 mm would require a general 3D rather than an axi-symmetric implementation of the present model. Indeed a 3D formulation of the present approach will also be required to model the motion of more than one bubble. This retains the computation cost advantages of a boundary element formulation although it will be necessary to formulate models to handle bubble collisions that may lead to rebound or coalescence.

In summary:

- The current model predicts the shape, velocity and transient behaviour of a rising bubble without fitting parameters.
- The good quantitative agreement between theoretical predictions and experimental observations suggests that the constructed model is basically correct and has encompassed the essential physical elements that determine bubble rise and deformation.
- It also strongly suggests that the wake of the bubble is not a primary determinant of the dynamics of the bubble. Instead the dynamics are mainly controlled by potential flow where the viscous effects enter through the boundary condition.
- The model as presented here provides a resolution to the d'Alembert [44] paradox for the rising bubble problem (which led to the remark "… résistance nulle. Ce qui est absurde." by d'Alembert) while avoiding the need for complex numerical computations.

Acknowledgements

This work is supported in part by the Australian Research Council. D.Y.C.C. is an Adjunct Professor at the National University of Singapore.

References

[1] Loth E. Quasi-steady shape and drag of deformable bubbles and drops. Int J Multiphase Flow 2008;34:523–46.
[2] Magnaudet J, Eames I. The motion of high-Reynolds-number bubbles in inhomogeneous flows. Annu Rev Fluid Mech 2000;32:659–708.
[3] Clift R, Grace JR, Weber ME. Bubbles, drops and particles. Academic Press; 1978.
[4] Hadamard JS. Mouvement permanent lent d'une sphère liquide et visqueuse dans un liquide visqueux. C R Acad Sci 1911;152:1735–43.
[5] Levich VG. Motion of gas bubbles with high Reynolds numbers. Zh Eksp Teor Fiz 1949;19:18–24.
[6] Ackeret J. Über exakte Lösungen der Stokes–Navier-Gleichungen inkompressibler Flüssigkeiten bei veränderten Grenzbedingungen. Z Angew Math Phys 1952;3:259–71.
[7] Chan BKC, Prince RGH. Distillation studies—viscous drag on a gas bubble rising in a liquid. AIChE J 1965;11:176–92.
[8] Mei R, Klausner JF, Lawrence CJ. A note on the history force on a spherical bubble at finite Reynolds number. Phys Fluids 1994;6:418–20.
[9] Moore DW. The boundary layer on a spherical gas bubble. J Fluid Mech 1963;16:161–76.
[10] Malysa K, Krasowska M, Krzan M. Influence of surface active substances on bubble motion and collision with various interfaces. Adv Colloid Interface Sci 2005;114–115:205–25.
[11] Duineveld PC. The rise velocity and shape of bubbles in pure water at high Reynolds number. J Fluid Mech 1995;292:325–32.
[12] Wu M, Gharib M. Experimental studies on the shape and path of small air bubbles rising in clean water. Phys Fluids 2002;14:49–52.
[13] Okazaki S. The velocity of ascending air bubbles in aqueous solutions of a surface active substance and the life of the bubble on the same solution. Bull Chem Soc Japan 1964;37:144–50.
[14] Zhang Y, Finch JA. A note on single bubble motion in surfactant solutions. J Fluid Mech 2001;429:63–6.

[15] Parkinson L, Sedev R, Fornasiero D, Ralston J. The terminal rise velocity of 10−100 μm diameter bubbles in water. J Colloid Interface Sci 2008;322:168–72.
[16] Ryskin G, Leal LG. Numerical solution of free-boundary problems in fluid mechanics. Part 2. Buoyancy-driven motion of a gas bubble through a quiescent liquid. J Fluid Mech 1984;148:19–35.
[17] Yang B, Prosperetti A, Takagi S. The transient rise of a bubble subject to shape or volume changes. Phys Fluids 2003;15:2640–8.
[18] Hua J, Stene JF, Lin P. Numerical simulation of 3D bubbles rising in viscous liquids using a front tracking method. J Comput Phys 2008;227:3358–82.
[19] Hua J, Lou J. Numerical simulation of bubble rising in viscous liquid. J Comput Phys 2007;222:769–95.
[20] Scardovelli R, Zaleski S. Direct numerical simulation of free-surface and interfacial flow. Annu Rev Fluid Mech 1999;31:567–603.
[21] Prosperetti A, Tryggvason G. Computational methods for multiphase flows. Cambridge University Press; 2007.
[22] Miksis LM, Vanden-Broeck J-M, Keller JB. Rising bubbles. J Fluid Mech 1982;123:31–41.
[23] Boulton-Stone JM, Robinson PB, Blake JR. A note on the axisymmetric interaction of pairs of rising, deformable gas bubbles. Int J Multiphase Flow 1995;21:1237–41.
[24] Blake JR, Boulton-Stone JM, Tong PR. Boundary integral methods for rising, bursting and collapsing bubbles. In: Power H, editor. BE applications in fluid mechanics, vol. 4. Southampton, UK: Computational Mechanics; 1995. p. 31–72.
[25] Lundgren TS, Mansour NN. Oscillations of drops in zero gravity with weak viscous effects. J Fluid Mech 1988;194:479–510.
[26] Joseph DD. Potential flow of viscous fluids: historical notes. Int J Multiphase Flow 2006;32:285–310.
[27] Joseph DD, Wang J. The dissipation approximation and viscous potential flow. J Fluid Mech 2004;505:365–77.
[28] Batchelor GK. An introduction to fluid dynamics. Cambridge University Press; 1967.
[29] Kang IS, Leal LG. The drag coefficient for a spherical bubble in a uniform streaming flow. Phys Fluids 1988;31:233–7.
[30] Blake JR, Taib BB, Doherty G. Transient cavities near boundaries. Part 1. Rigid boundary. J Fluid Mech 1986;170:479–97.
[31] Chesters AK. An analytical solution for the profile and volume of a small drop or bubble symmetrical about a vertical axis. J Fluid Mech 1977;81:609–24.
[32] Klaseboer E, Hung KC, Wang C, Wang CW, Khoo BC, Boyce P, Debono S, Charlier H. Experimental and numerical investigation of the dynamics of an underwater explosion bubble near a resilient/rigid structure. J Fluid Mech 2005;537:387–413.
[33] Lee M, Klaseboer E, Khoo BC. On the boundary integral method for the rebounding bubble. J Fluid Mech 2007;570:407–29.
[34] Khoo BC, Klaseboer E, Hung KC. A collapsing bubble-induced micro-pump using the jetting effect. Sensors Actuators A 2005;118:152–61.
[35] Klaseboer E, Fong SW, Turangan CK, Khoo BC, Szeri AJ, Calvisi ML, et al. Interaction of lithotripter shockwaves with single inertial cavitation bubbles. J Fluid Mech 2007;593:33–56.
[36] Borkent BM, Arora M, Ohl C, De Jong N, Versluis M, Lohse D, et al. The acceleration of solid particles subjected to cavitation nucleation. J Fluid Mech 2008;610:157–82.
[37] Fong SW, Klaseboer E, Turangan CK, Khoo BC, Hung KC. Numerical analysis of a gas bubble near bio-materials in an ultrasound field. Ultrasound in Med Biol 2006;32:925–42.
[38] Longuet-Higgins MS, Cokelet ED. The deformation of steep surface waves on water I. A numerical method of computation. Proc R Soc London A 1976;350:1–26.
[39] Wang QX, Yeo KS, Khoo BC, Lam KY. Strong interaction between a buoyancy bubble and a free surface. Theort Comput Fluid Dyn 1996;8:73–88.
[40] Schiller L, Naumann A. Über die grundlegenden Berechnungen bei der Schwerkraftaufbereitung. Zeit Ver Deut Ing 1933;77:318–20.
[41] Moore DW. The velocity of rise of distorted gas bubbles in a liquid of small viscosity. J Fluid Mech 1965;23:749–66.
[42] Brennen CE. Fundamentals of multiphase flows. Cambridge University Press; 2005.
[43] Klaseboer E, Khoo BC. A modified Rayleigh–Plesset model for a non-spherically symmetric oscillating bubble with applications to boundary integral methods. Eng Anal Bound Elem 2006;30:59–71.
[44] d'Alembert J. Essai d'une nouvelle théorie de la résistance des fluides, Paris, 1752.